Hyperballistic intercellular signaling through growth assisted positive feedback

Meidi Wang[1], Louis González[2], Soutick Saha[3], Krešimir Josić[4,5,6,7], Andrew Mugler[2*], Matthew R. Bennett[4,7,8*]

[1]PhD Program in Systems, Synthetic, and Physical Biology, Rice University, 6100 Main St., Houston, TX, 77005, USA.
[2]Department of Physics and Astronomy, University of Pittsburgh, 3941 O'Hara St, Pittsburgh, 15260, Pennsylvania, USA.
[3]Department of Physics and Astronomy, Purdue University, 525 Northwestern Ave, West Lafayette, 47907, Indiana, USA.
[4]Department of Biosciences, Rice University, 6100 Main St., Houston, TX, 77005, USA.
[5]Department of Mathematics, University of Houston, 4800 Calhoun Blvd, Houston, 77204, TX, USA.
[6]Department of Biology and Biochemistry, University of Houston, 4800 Calhoun Blvd, Houston, 77204, TX, USA.
[7]Rice Synthetic Biology Institute, Rice University, 6100 Main St., Houston, TX, 77005, USA.
[8]Department of Bioengineering, Rice University, 6100 Main St., Houston, TX, 77005, USA.

*Corresponding author(s). E-mail(s): andrew.mugler@pitt.edu; matthew.bennett@rice.edu;
Contributing authors: mw73@rice.edu; gonzalezlouis@pitt.edu; soutick2010@gmail.com; josic@math.uh.edu;

Abstract

Intercellular signaling in bacteria is often mediated by small molecules secreted by cells. These small molecules disperse via diffusion which limits the speed and spatial extent of information transfer in spatially extended systems. Theory shows that a secondary signal and feedback circuits can speed up the flow of information and allow it to travel further. Here, we construct and test several

synthetic circuits in *Escherichia coli* to determine to what extent a secondary signal and feedback can improve signal propagation in bacterial systems. We find that positive feedback-regulated secondary signals propagate further and faster than diffusion-limited signals. Additionally, the speed at which the signal propagates can accelerate in time, provided the density of the cells within the system increases. These findings provide the foundation for creating fast, long-range signal propagation circuits in spatially extended bacterial systems.

Keywords: intercellular signaling, trigger wave, synthetic biology

1 Introduction

Intercellular signaling plays an essential role in both unicellular and multicellular organisms. Intercellular communication in multicellular organisms is critical for coordinating cell differentiation during development [1],[2]. In unicellular organisms, such as bacteria or yeast, intercellular signaling can help colonies synchronize their behavior to improve survival in challenging and changing environments [3],[4],[5],[6]. In synthetically engineered multicellular systems, intercellular communication plays a central role in the emergence of programmed spatiotemporal patterns within the population [7],[8],[9],[10].

In bacteria, intercellular signals are mediated by a variety of molecules[11], such as acyl-homoserine lactones[12], quinolones[13], and nitric oxide[14] that, once secreted or transported out of a cell, diffuse through the extracellular space. Although diffusion is fast and reliable across distances on the order of the size of a single cell, it becomes inefficient for propagating information at millimeter or centimeter scales[15]. At large distances diffusion is relatively slow, and the strength of the signal (*i.e.* its local concentration) rapidly decreases as a function of distance from the source(Fig. 1a).

Cells can overcome the limitations of diffusion and coordinate behavior over large distances by combining intercellular signaling mechanisms with positive feedback to create spatial trigger waves[16]. Such waves maintain their amplitude and speed during signal propagation [17],[18],[19] (Fig. 1b). While spatial trigger waves are typically associated with metazoans, similar mechanisms may play a role in signal propagation in bacterial quorum sensing (QS) [20],[21]. These quorum sensing systems are important for sensing cell density, but may also be used for mediating intracellular communication in spatially heterogeneous environments [21],[22],[23],[24]. Studies have suggested that autoinducer diffusion, coupled with positive feedback-regulated autoinducer synthesis, facilitates signal propagation in a traveling wave fashion [20],[25],[26]. Indeed, experiments have shown that distant cells are activated when local QS molecules are supplied exongenously [21],[27],[28],[29].

However, while spatial trigger waves have been shown to provide a mechanism for long-range communication [18],[19], their ability to facilitate rapid, long-distance signaling in bacteria remains unexplored. Signal propagation through gene expression is

inherently coupled with bacterial growth and division [21],[27],[30],[31]. The exponential growth of bacteria may act as an amplifier of signal propagation as cell density increases. On the other hand, once cells reach stationary phase they exhibit sharply reduced growth and gene expression, damping both the production and amplification of intercellular signals (Fig. 1c,d). Autoinducers have been shown to accelerate the diffusing signal front [21],[27], but only when added exogenously to the bacteria performing quorum sensing. As population size increases, the self-activation of autoinducers complicates the ability to distinguish whether true signal propagation is occurring or if the system is merely being triggered by reaching a population threshold [21]. Thus, a new experimental approach and an accompanying theoretical framework are needed to understand the complex interplay between cellular population growth, gene expression, and signal transmission.

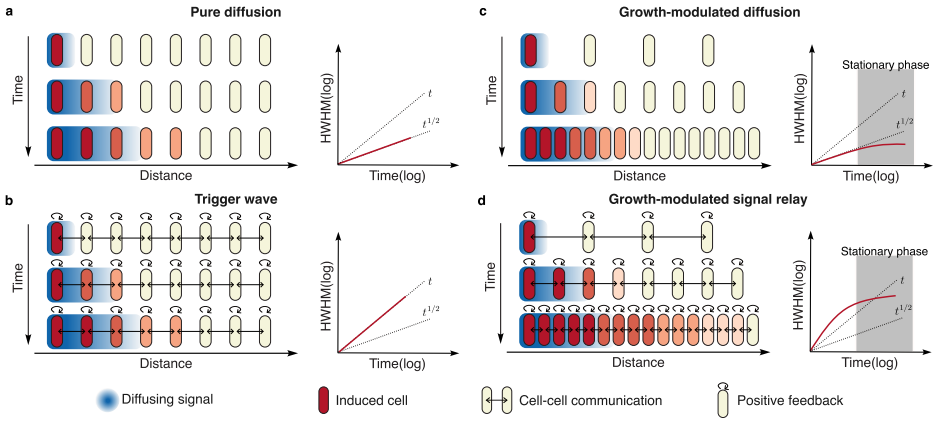

Fig. 1: Conceptual illustration of how bacteria respond to a local signal. (**a**) Pure diffusion: The signal diffuses as a gradient (blue) and activates a cellular response (red). Half-Width Half-Maximum (HWHM), the distance from the maximum signal response to the point where the signal response falls to half of its maximum value, represents the extent of signal propagation. Cells show a diminishing response over time and distance. (**b**) Trigger wave: Incorporates both spatial coupling and feedback loops, as indicated by arrows between and within cells. Each induced cell (red) stimulates neighboring cells, thereby maintaining a constant signal propagation speed. (**c**) Growth-modulated diffusion: Similar to pure diffusion but includes the impact of cell growth dynamics on signal propagation. The signal propagates similarly to pure diffusion and stops as cells approach the stationary phase. (**d**) Growth-modulated signal relay: A combination of cell growth and intercellular positive feedback. Active cell growth accelerates signal propagation before it slows down when cells enter stationary phase.

To investigate the role of positive feedback in long-range intercellular signaling in growing bacterial communities, we constructed a synthetic signal relay system in *E. coli* that uses positive feedback to amplify and relay signals as they propagate through a spatially extended community. This bottom-up approach allowed us to

systematically probe each component of the signaling system to determine how they affect a community's response to a spatially localized input signal. Importantly, the positive feedback in our engineered bacteria does not lead to self-activation at high cell densities. This is in contrast to QS systems found in nature that, due to leaky expression of the AHL synthase, auto-activate at large cell densities[24]. We could thus decouple diffusion and feedback-mediated signal propagation from population mediated signal activation.

We found that *E. coli* with a positive feedback-coupled intercellular signaling system exhibited super-diffusive signal propagation, and that such propagation was not possible when either the feedback or the intercellular signaling was removed. Furthermore, we found that the propagation was enhanced beyond the expected ballistic regime by the exponential growth of the cells themselves, and that the propagation rate could be tuned by altering the duration of the exponential growth phase (Fig. 1d). A mathematical model explained why both feedback and intercellular signaling are required for robust super-diffusive propagation, and it revealed how exponential cell growth can lead to hyperballistic signal propagation (*i.e.* signals that accelerate with time). We thus demonstrate that a bacterial colony can overcome the short length scales of diffusive communication using positive feedback and intercellular signaling, and can surpass even ballistic propagation by coupling signaling and population growth.

2 Results

2.1 Growth-modulated signal relay

To investigate the roles of growth and feedback on intercellular signaling, we engineered a strain of *E. coli* (IS+PF+) that responds to an externally applied input signal (erythromycin) and uses a secondary signal (C4 homoserine lactone, C4-HSL) and feedback control to spatially propagate the response throughout the population (Fig. 2a). The addition of erythromycin de-represses the P_{mph} promoter which drives expression of *rhlI*[32], a gene encoding the acyl-homoserine lactone synthase, RhlI. When present, RhlI produces C4-HSL, a small molecule that freely diffuses in and out of cells and binds to the transcriptional activator RhlR to up-regulate transcription from P_{rhl} promoters [33]. To incorporate positive feedback without causing self-activation, we utilized a leak-dampener module previously developed by Ho et al.[34]. This module, driven by P_{rhl}, includes a second copy of the *rhlI* gene, denoted as *rhlI.2TAG*, with the first two leucine codons mutated to amber stop codons (TAG), and the leucine suppressor tRNA *supP*. In the absence of C4-HSL, the translation of *rhlI.2TAG* is significantly reduced by the stop codons. In the presence of C4-HSL, *supP* enables translation of *rhlI.2TAG*, which produces more C4-HSL. Both RhlI and RhlI.2TAG contain C-terminal ssrA degradation tags that target the ClpXP protease [35]. An additional copy of P_{rhl} drives expression of the gene encoding superfolder yellow fluorescent protein (sfYFP), which we use to monitor the response of the cells. *mphR* and *eryR* are in the same expression cassette controlled by the constitutive promoter

P_{lacIq}[32]. The plasmids containing this circuit were transformed into *E. coli* strain CY027 with *rhlR* encoded in the genome [8].

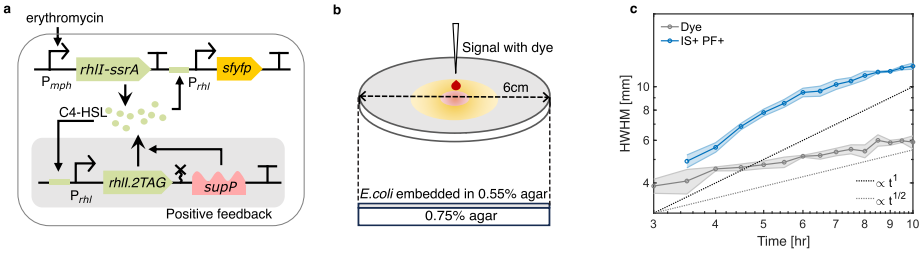

Fig. 2: (**a**) Circuit diagram of the sigal relay strain (IS+PF+). Erythromycin increases C4-HSL production via the RhlI synthase. C4-HSL induces the expression of *sfyfp*, *rhlI.2TAG*, and the transcription of*supP*. The *rhlI.2TAG* has two leucine codons replaced by amber stop codon TAG. Increased transcription of *supP* allows for more *rhlI* expression by mediating correction translation of leucin codons. (**b**) Schematic of experiment design illustrating cell culture in solid medium and application of exogenous signal. (**c**) Measured wavefront dynamics (half width half maximum HWHM) of the growth-modulated IS+PF+ strain and the dye. Shaded region corresponds to one standard deviation of triplicates. Both axes are set to a logarithmic scale.

We next confirmed that the IS+PF+ strain can respond to an external erythromycin signal and report with *sfyfp* expression. We tested the strain in liquid culture across a range of erythromycin concentrations (Supplementary Fig. 1a). As expected, higher concentrations of erythromycin resulted in increased sfYFP expression (Supplementary Fig. 1a). The addition of erythromycin induced fluorescence expression without affecting the growth rate. To ensure that positive feedback does not cause self-activation in the absence of erythromycin, we grew the IS+PF+ strain in liquid and solid media and compared its fluorescence with two control strains – one with intercellular signaling but without positive feedback (IS+PF-), and another with intercellular signaling but lacking the leak dampener systems (IS+PF+LD-). Similar to the IS+PF+ strain, the IS+PF- strain contains the P_{mph} promoter driving expression of *rhlI* and the P_{rhl} promoter driving expression of *sfyfp*. However, the IS+PF- strain does not contain the *rhl.2TAG* and hence there is no positive feedback on *rhl* expression. Note that the second copy of the P_{rhl} promoter still drives transcription of *supP*. When grown in LB broth and soft LB agar, the fluorescence levels of both IS+PF+ strain and IS+PF- strain were comparable, suggesting no self-activation was introduced by the leak dampened positive feedback. In contrast, the IS+PF+LD- strain exhibited high levels of fluorescence, indicating self-activation (Supplementary Fig. 1b). Together, these results confirm that the IS+PF+ strain is tunable with erythromycin and does not exhibit self-activation due to the positive feedback loop.

To determine if the IS+PF+ strain can propagate erythromycin signals faster than diffusion, we embedded exponentially-growing cells into 0.55% soft-agar and applied erythromycin with a red fluorescence dye (Sulforhodamine 101) to the center of the

plate (Fig. 2b). We recorded the fluorescence on the plate every 30 minutes for 10 hours after inoculating the cells (see Methods). Figure 2c showed that the wavefront of sfYFP in the IS+PF+ strain outpaced the wavefront of the dye (as measured by the half-width half-maximum (HWHM) of the signal). As expected for a diffusive molecule, the diffusion of the dye led to an increases in wavefront distance proportional to the square root of the elapsed time. In contrast, the wavefront of sfYFP traveled approximately linearly with time before eventually slowing down.

We hypothesized that the slowdown observed at later times occurred due to cells entering stationary phase, which is characterized by nutrient or space depletion leading to, among other effects, an equilibium between cell division and cell death and changes in gene expression [36],[37]. During stationary phase, *E. coli* activates gene expression related to maintenance of resource and energy for survival and downregulates other metabolic activities, resulting in reduced production of C4-HSL and sfYFP. We verified the growth phase of cells on agar plate by measuring the cell density change over the course of the experiment and confirmed that cell density saturated around five hours after we seeded them in agar, suggesting a growth phase shift (Supplementary Fig. 2).

2.2 Minimal ingredients for signal relay

We next asked whether both intercellular signaling and positive feedback are necessary for signals to propagate faster than diffusion. To answer this question, we created two new circuits – one incorporating positive feedback, but lacking intercellular signaling (IS-PF+), and one lacking both intercellular signaling and positive feedback (IS-PF-). For the IS-PF+ circuit, the P_{mph} promoter controls the expression of the gene encoding the transcriptional activator *araC* instead of *rhlI*. AraC, when bound to arabinose, activates its target promoter (P_{BAD})[38] and, importantly, does not synthesize a diffusible signaling molecule like RhlI does. Abundant arabinose is provided in the system. There are two copies of P_{BAD}, one driving expression of the reporter *sfyfp* and the other driving expression of a leak-dampened version of *araC*, *araC.2TAG*. Both AraC and AraC.2TAG contain C-terminal ssrA degradation tags that target the ClpXP protease[35]. The IS-PF- circuit contains neither intercellular signalling nor positive feedback. This circuit contains the P_{mph} promoter driving expression of *araC* and two copies of P_{BAD}, one driving *sfyfp* and the other *supP* (without *araC.2TAG*). We measured the response of the four circuits to various erythromycin concentrations in liquid culture (Supplementary Fig. 1a). All strains showed similar sensitivity to erythromycin. The strains with positive feedback exhibited higher maximum fluorescence while maintaining low basal expression, suggesting low self-activation. The basal expression level of the IS-PF+ strain was also confirmed in soft LB agar. The fluorescence level of the IS-PF+ strain was similar to the fluorescence level of the IS-PF- strain (Supplementary Fig. 1b).

After confirming that each of the four strains functions properly in a homogeneous environment, we performed signal propagation assays as described above. Exponentially growing cells were embedded in soft agar and erythromycin deposited at the center of the plate. Time-lapse images showed that the IS-PF- strain exhibited the lowest fluorescence, due to a weaker fluorescence expression cassette (Fig. 3a). The IS+PF- strain exhibited substantially higher fluorescence, although it showed similar

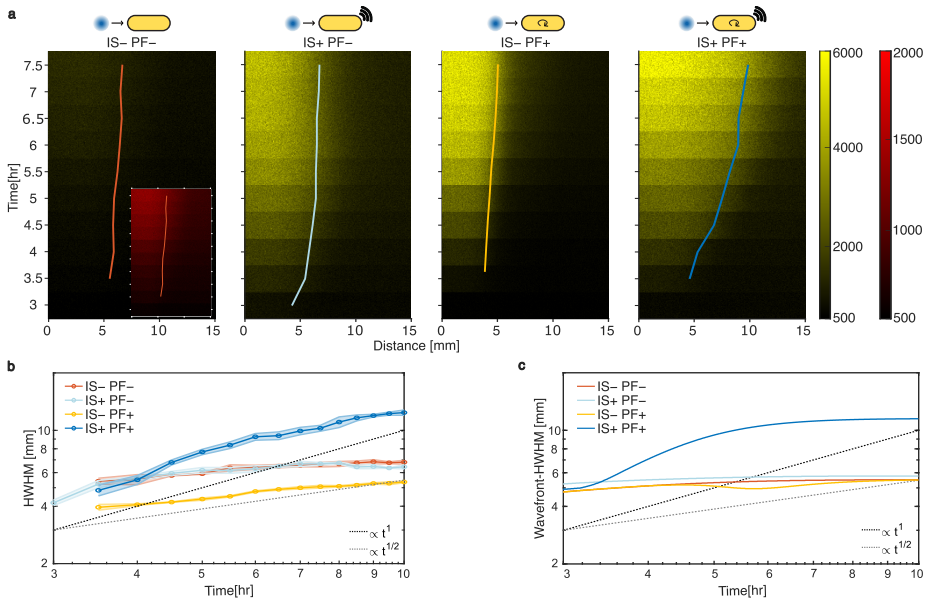

Fig. 3: (**a**) Time-lapse montage of sfYFP in the IS-PF- strain, the IS+PF- strain, the IS-PF+ strain, and the IS+PF+ strain. Fluorescence intensities are normalized to the same maximum and minimum values. The inset shows the IS-PF- strain with fluorescence intensities normalized to lower maximum values, represented by the red color bar on the right. (**b**) Measured wavefront dynamics (HWHM) in four strains. Shaded region corresponds to one standard deviation of triplicates. Both axes are set to a logarithmic scale.(**c**) Simulated wavefront dynamics. The simulation parameters are listed in Supplementary Table 1. The model and experiment data qualitatively agree. Both demonstrate the super-diffusive signal propagation in the IS+PF+ strain and diffusive propagation in the IS-PF- strain, IS+PF- strain and IS-PF+ strain.

levels of sfYFP expression to the IS-PF- strain in liquid culture (Supplementary Fig. 1a). The difference in fluorescence between liquid and solid media was due to the fast dilution of C4-HSL in liquid media caused by the circular shaking motion of liquid media[39],[40]. This faster dilution led to lower activation of the P_{rhl} promoter than the same cells in solid media.

Signal propagation that relies solely on erythromycin faces the same limitations as the dye: the distance increases as the square root of time. To determine whether both intercellular signaling and positive feedback are necessary for the super-diffusive propagaion of signals we observed, we measured the wavefront movements in each of the four strains. The IS+PF+ strain displayed elevated fluorescence expression at a substantially larger distance from the diffusing source (Fig.3a,b). The wavefront distance in the IS-PF- strain increased as the square root of time, consistent with erythromycin diffusion. The IS-PF+ strain showed higher fluorescence than the IS-PF- strain due to positive feedback. However, the wavefront distance in the IS-PF+ strain still increased as the square root of time, and the distance of the IS-PF+ strain was smaller than

the IS-PF- strain. This can be explained by the increased fluorescence intensity at the diffusing source in the IS-PF+ strain. Although positive feedback amplified *sfyfp* expression, this amplified response did not spread to neighboring cells due to the lack of intercellular signaling. The wavefront distance in the IS+PF- strain also increased as the square root of time. The IS+PF- cells respond to erythromycin with C4-HSL production, which activates *sfyfp* expression. Although C4-HSL diffusion smoothed the transition between activated and nonactivated cells, its limited diffusion restricted the overall propagation. The IS+PF+ cells in the experiment exhibited super-diffusive signal propagation, overcoming the limitation of erythromycin diffusion.

2.3 A mathematical model of signal propagation

To provide a mechanistic understanding of the experimental results, and explain and predict the impact of changes in experimental conditions, we developed a mathematical model of the engineered system. We modeled the propagation of signaling molecules and the cellular responses using a system of partial differential equations (PDEs). Working in polar coordinates, and acknowledging the angular symmetry of the bacterial colony, we write the PDEs in terms of the radial coordinate, r, measuring the distance from the center of the population. These equations describe the concentration of the diffusing source, erythromycin (s), that induces production of either AraC or C4-HSL (z), which then produces the readout, sfYFP (y). The dynamics of these concentrations are described by

$$\frac{\partial s}{\partial t} = D\left(\frac{1}{r}\frac{\partial s}{\partial r} + \frac{\partial^2 s}{\partial r^2}\right), \tag{1}$$

$$\frac{\partial z}{\partial t} = F_i(s, z), \tag{2}$$

$$\frac{\partial y}{\partial t} = f_i(t)\phi z, \tag{3}$$

with initial condition $s(r, t = 0) = s_0\Theta(r < R_0)$ and $z(r, 0) = y(r, 0) = 0$, where s_0 is the initial concentration of erythromycin, R_0 sets the radius of the initial droplet of erythromycin added to the medium, and Θ denotes the Heaviside step function. In equation (1), the right-hand side is the radial part of the Laplacian in polar coordinates with D the diffusion constant of erythromycin, and ϕ is an activation strength of y (sfYFP) by z (either araC or rhlI).

In equation (2), the function $F_i(s, z)$ captures the activation and feedback in each of the four strains. Specifically, in the IS-PF- case, $F_1(s, z) = f_1(t)a_1 s^{H_1}/(s^{H_1} + s_1^{H_1})$ models the activation of araC by erythromycin, with activation strength a_1, Hill coefficient H_1, and half-maximal concentration s_1. In the IS-PF+ case, $F_2(s, z) = f_2(t)[a_1 s^{H_1}/(s^{H_1} + s_1^{H_1}) + a_1 b_2 z^{J_2}/(z^{J_2} + z_2^{J_2})]$ models both activation and feedback of AraC, with relative feedback strength b_2, Hill coefficient J_2, and half-maximal concentration z_2. We assumed that the activation parameters a_1, H_1, and s_1 are equal in the case of the IS-PF- and IS-PF+ strain because the activation components have the same molecular construction. In the IS+PF- case, $F_3(s, z) = f_3(t)a_3 s^{H_3}/(s^{H_3} + s_3^{H_3}) + E[(\partial z/\partial r)/r + \partial^2 z/\partial r^2]$ models the activation and diffusion of C4-HSL, which

is synthesized by rhlI, with diffusion coefficient E. Finally, in the IS+PF+ case, $F_4(s,z) = f_4(t)[a_3 s^{H_3}/(s^{H_3} + s_3^{H_3}) + a_3 b_4 z^{J_4}/(z^{J_4} + z_4^{J_4})] + E[(\partial z/\partial r)/r + \partial^2 z/\partial r^2]$ models the activation, feedback, and diffusion of C4-HSL. We again assumed that the activation parameters a_3, H_3, and s_3 equal for the IS+PF- and IS+PF+ strain because the induced production of C4-HSL by erythromycin are identical.

In equations (2) and (3), protein production is modulated by an envelope function, $f_i(t)$. This function reflects the fact that the rate of protein production is modulated by the rate of cell growth [30]. Specifically, we assume the growth envelope function $f_i(t) = \sqrt{n_i \dot{n}_i / g_i C_i^2}$ (Methods) where $n_i(t)$ is the cell number, g_i is the growth rate of the cells, and C_i is the carrying capacity for a given circuit i. We assume that the number of cells per unit volume in the population grows logistically with a lag phase [41], and has the form

$$n_i(t) = \frac{n_{0,i}}{\left(\frac{C_i - n_{0,i}}{n_{0,i}}\right) e^{g_i B_i(t)} + 1} \tag{4}$$

where $n_{0,i}$ is the initial cell number and

$$B_i(t) = t + \frac{1}{\alpha} \ln\left(\frac{e^{-\alpha(t-\lambda_i)}}{e^{\alpha\lambda_i} + 1}\right) \tag{5}$$

quantifies the cell growth from an initial lag phase with lag time λ_i.

We obtained the parameters in equations (1-5) directly from our experimental measurements (R_0, s_0, g_i, $n_{0,i}$, C_i, λ_i, a_i, H_i, and s_i) or from the literature (D and E), as described in the Methods. Where this was not possible (J_i, z_i, and b_i), we explored the effects of these remaining parameters on the propagation dynamics and calibrated the parameters to the experimental dynamics (Methods). We also explored a version of the model with degradation of the intermediate (AraC is actively degraded whereas C4-HSL is not) and found that such degradation does not significantly affect the results (Methods). All parameter values are listed in Supplementary Table 1.

We found that the mathematical model produces dynamic concentration profiles of sfYFP for all four strains (Supplementary Fig. 3) that agree qualitatively with those measured in the experiments (Fig. 3a). In particular, the model recapitulates the faster and longer signal propagation in the IS+PF+ compared to the other three strains. Figure 3c shows the HWHM propagation curves from the model, and we see excellent agreement with experimentally obtained propagation curves in Figure 3b.

Having a model that successfully captures the propagation dynamics provides evidence that the qualitative features found in the simulations are congruent with the experiments. The model shows that in the absence of positive feedback, intercellular signaling alone is not sufficient to produce super-diffusive signal propagation. To elucidate the physical mechanism responsible for the differences in signal propagation between the four strains we performed a linear analysis of the model (Supplementary). We found that in the models of the IS-PF- and IS+PF- strains signals always propagate diffusively ($\propto t^{1/2}$). In the model IS-PF+ strain signals can propagate super-diffusively in certain specialized parameter regimes, even as the signal becomes weak due to its own diffusion. Only the IS+PF+ strain model allows for a robust, ballistic signal propagation ($\propto t$). This finding helps explain why the IS+PF+ strain

exhibited much faster propagation dynamics than the other three strains in both the experiments (Figure 3b) and numerical simulations (Figure 3c).

Further, linear analysis of the model (Supplementary) reveals how cell growth, by increasing the amplitude of the signal profile over time, couples the propagation dynamics to the growth dynamics, leading to hyperballistic propagation in the IS+PF+ case. This finding helps explain the regime in Figure 3b and c where the IS+PF+ strain exhibits propagation dynamics (blue) that are slightly faster than ballistic (slope larger than 1 on the log-log scale) and suggests predictions for how to enhance this regime. We investigated these and other predictions next.

2.4 Tuning the signal propagation dynamics

The PDE model makes several predictions about how the signalling dynamics can be tuned. First, the model predicts that increasing the initial concentration of erythromycin yields an increase of responder protein (either AraC or RhlI) and thus an increase of sfYFP (Supplementary Fig. 4a). To test this, we performed further experiments by using various signal concentrations in our propagation assay. Consistent with the model prediction, we observed an increasing signaling distance with increasing input signal concentration, while the signal propagation rate remained constant regardless of the signal concentration (Supplementary Fig. 4b).

Next, the linearized model predicts that signal propagation of the IS+PF+ strain can accelerate in time, provided cells are growing exponentially (Supplementary). Therefore, we investigated if extending the exponential phase of cell growth would lead to more hyperballistic signal propagation. We calibrated the growth parameters of the model ($n_{0,i}$, g_i, C_i, and λ_i) with the measured cell densities over time when we seeded cells at different initial densities (Supplementary Table 2). The numerical results also predicted that the IS+PF+ strain would show hyperballistic signal propagation with low initial cell density, whereas the IS-PS- strain, the IS+PF- strain and the IS-PF+ strain would always exhibit diffusive signal propagation (Fig. 4a-b and Supplementary Fig. 5a-b).

To experimentally verify these model predictions, we seeded the cells at different initial densities to modulate the growth phase of cells on agar. As the nutrient and space remained the same, populations with a smaller initial size underwent an extended exponential phase compared to populations with a larger initial size[42],[43]. We seeded cells at three different initial densities (optical density (OD) = 0.2, 0.6 and 1.8) and measured the growth dynamics of cells on agar plates using a series of plating assays, as described in the methods section. As expected, cells seeded with a lower initial density reached the stationary phase approximately an hour later than cells seeded at higher cell densities (Supplementary Fig. 2). The agar plates with lower initial density exhibited observable fluorescence signals 30 minutes to 1 hour later than plates with higher density due to the measuring limitation of the microscope. Varying the initial cell density, consistent with model predictions, we found that the signaling distance and propagation rate was similar across all three initial densities in the IS-PS- strain, the IS+PF- strain and the IS-PF+ strain (Fig. 4c, Supplementary Fig. 5c-d). In contrast, the IS+PF+ strain exhibited an increase of the hyperballistic signal

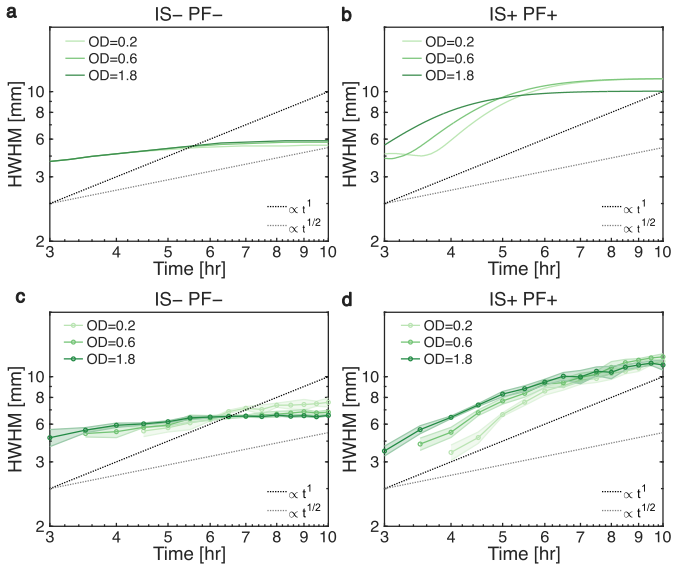

Fig. 4: Growth modulated wavefront propagation (HWHM) (**a-b**)Simulated wavefront dynamics with different initial densities for the IS-PF- strain and the IS+PF- strain. (**c-d**) Measured wavefront dynamics (HWHM) of the IS- PF- and the IS+ PF+ strain with three different initial seeding densities (optical density = 0.2, 0.6 and 1.8). Shaded region corresponds to one standard deviation of triplicates. Both axes are set to a logarithmic scale.

propagation phase with decreasing OD (Fig. 4d). The enhancement is particularly pronounced with initial OD = 0.2 at 4 to 6 hours.

The IS+PF+ strain not only exhibited increased signaling distance but also demonstrated enhanced propagation speed when coupled with exponential growth. These results confirmed that signal relay is achieved through the incorporation of both positive feedback and intercellular signaling elements, and enhanced further by cell growth.

2.5 Wavefront measured by threshold

In biological systems the half-width-half-maximum (HWHM) is not always the most meaningful measure of wavefront location. This is because the wavefront often needs to trigger a downstream component that requires a minimum concentration to activate[44],[45]. In our system, this could correspond to the output (sfYFP) representing a transcription factor (TF) that upregulates or downregulates a downstream promoter. To account for this, we reanalyzed our data using an arbitrary threshold to measure the position of the wavefront. In other words, we measured the fluorescence per cell at each position and compared it to an arbitrary value. The position of the wavefront was then determined by the furthest point from the signal source at which the fluorescence per cell was greater than or equal to the threshold value. Note

that the fluorescence must be scaled by the time dependent cell density in order to approximate the concentration of protein per cell.

We quantified the wavefront dynamics over time for all four strains using 10% of the maximum fluorescence of the corresponding strain as the threshold. As with the wavefront measured using HWHM, the signal propagation of the IS+PF+ strain was super-diffusive, while the other three strains remained diffusive (Fig. 5a). In the context of regulating downstream promoters, the relevant TF threshold varies depending on promoter properties, such as the binding affinity of the TF to the promoter. To assess whether the signal propagation dynamics remain consistent when changing the threshold, we quantified the wavefront dynamics using thresholds ranging from 10% to 50% of the maximum fluorescence. As expected, the wavefront distances decreased with increasing thresholds. However, the signal propagation speed of the IS+PF+ strain remained constant regardless of the threshold, while the other three strains showed decreasing speeds over time (Supplementary Fig. 6).

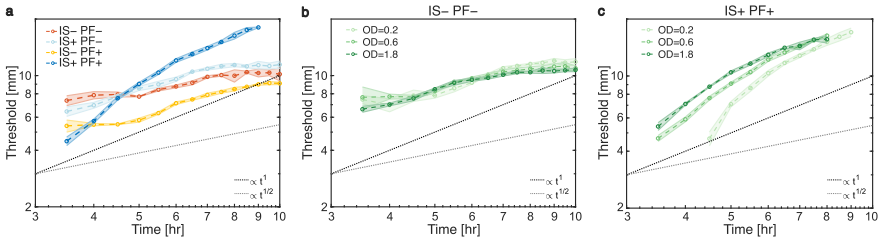

Fig. 5: Growth modulated wavefront propagation (scaled threhold) (**a**) Measured wavefront dynamics (scaled threshold) for all strains. Shaded region corresponds to one standard deviation of triplicates. Both axes are set to a logarithmic scale. (**b-c**) Measured wavefront dynamics(scaled threshold) of the IS- PF- and the IS+ PF+ strain with three different initial seeding densities. Shaded region corresponds to one standard deviation of triplicates. Both axes are set to a logarithmic scale.

We also asked whether increasing signal propagation observed with exponentially growing cells was also observed when defining the wavefront using specific threshold values. We reanalyzed our data with varying initial cell densities and found consistent results: the IS+PF+ strain exhibited hyperballistic signal propagation when grown at low initial density, while propagaion in the IS-PF- strain, the IS-PF+ strain and the IS+PF- strain remained diffusive under all conditions (Fig. 5b-c, Supplementary Fig. 7). This result further demonstrated that we can modulate the signal propagation dynamics of the IS+PF+ strain by controlling its growth dynamics.

3 Discussion

In this work, we engineered a synthetic version of a trigger wave network in *E. coli* that is capable of transmitting information throughout a colony at super-diffusive speeds. Like its naturally occurring counterparts in multicellular organisms, signals in our system can travel with a constant speed. We also found that in our system signals

can actually accelerate and propagate hyper-ballistically. This is because the density of cells in our system can increase with time, and hence the propensity for the cells to sense and send signals at any given location can also increase. We showed that this phenomenon depends on the initial density of the cells (the longer the cells grow exponentially the faster the signal propagation), but the signalling speed might also be affected by other factors that influence growth, such as the growth medium and nutrient availability.

Of course, cellular growth has both positive and negative consequences for our system. On the plus side, growth can accelerate signaling and provide fast information transfer through the system. However, as cell density continues to increase, growth slows down and cells begin to enter stationary phase – leading to an overall slowdown of the signal as cells become less capable of responding. There are several ways in which this might be alleviated. For instance, stationary phase transcription is possible, using either phage polymerases[46],[47] or stationary phase promoters[48],[49]. However, we do not currently have as many tools to regulate these systems as we do exponential phase (σ^{70}) transcriptional systems[50],[51]. Another intriguing possibility, though, is to use engineered bacteria that do not grow or divide, but are still metabolically active[52]. When used in combination with our sginaling network, such "cyborg" bacteria could provide a means for long-term, and long-range responsiveness of cells to external stimuli.

It should be noted that while we embedded our engineered bacteria into agar, the same principles that guide our signalling networks should still hold for any material in which cells could be embedded that 1) supports some growth and 2) allows for extracellular signaling. Indeed, the integration of microbes with materials has given rise to a new class of engineered living materials[53] capable of sensing and responding to environmental signals[54]. The ability to coordinate distant cellular activity in response to local external stimuli will be essential in cases of stress and environmental changes. This module could be effectively incorporated into cellular circuits to enable fast, efficient, and long-range signal propagation in such living materials.

4 Methods

Plasmids and *E. coli* strain Plasmids of all strains were constructed using golden gate cloning methods. See Supplementary Table 3 for all plasmids used in this paper. All experiments were conducted in strain CY027 (*E. coli* BW25113 $\Delta lacI$ $\Delta araC$ $\Delta sdiA$ with constitutive *cinR* and *rhlR* integrated)[8].

Agar plate signal propagation assay *E. coli* strain CY027 containing the corresponding plasmids were cultured overnight at 37C with shaking at 250 rpm in LB medium containing both kanamycin (kan) and spectinomycin (spec). The saturated culture was diluted 200-fold into 30 mL of fresh LB medium with antibiotics and incubated at 37C with shaking at 250 rpm for less than 2 hours until their OD reached 0.2 to 0.3. Agar plates were prepared as follows: autoclaved 0.75% LB agar was melted and chilled to 55C in a water bath. Kan, spec, and arabinose were then added to the LB agar to a final concentration of 50 mg/L, 50 mg/L, and 0.1% (w/w), respectively. Next, 3.5 mL of well-mixed agar was aliquoted into each 60 mm petri dish to form

an even layer. 0.55% low-melt LB agar was melted and mixed with kan, spec, and arabinose, and kept warm in a 42C bath. Early exponential growth cells were concentrated and mixed with 0.55% low-melt LB agar to achieve a target final OD of 0.6 in all experiments unless specified otherwise. Then, 500 μL of the cell-agar mixture was aliquoted into the prepared petri dish with a layer of 0.75% LB agar. Each condition had three technical replicates. All plates were allowed to solidify at room temperature for 10 minutes. Next, 2 μL of the mixed solution containing erythromycin (2 mg/mL) and red fluorescent dye sulforhodamine 101(10 μg/ml) was deposited at the center of each plate. The cells were then incubated at 37°C for 10 hours. We imaged each plate under brightfield, yellow fluorescence, and red fluorescence every 30 minutes for up to 10 hours using a Nikon fluorescence stereo-microscope.

We compiled the yellow fluorescence images at different time points to create the images shown in Fig. 3a. Data analysis to measure the wavefront movement of each strain was performed with custom MATLAB code. This code determined the regions of interest (ROIs) using the red fluorescence images, which is a rectangle mask that is around 1000 pixels long from the center of the signal source to the edge of the field of view and 40 pixels wide. The radial yellow fluorescence profile at each time point was calculated by averaging the fluorescence along the width and subtracting the basal fluorescence intensity from the autofluorescence of E.coli and the LB media. This profile was noise-filtered by applying the Savitzky-Golay filter. The wavefront movement was calculated in two ways. The first method uses the half-width of a line shape at half of its maximum amplitude (HWHM) to represent the wavefront. The second method calculated the wavefront by normalizing the fluorescence profile by cell density and measuring the width of a line shape at a specific threshold L_{th}. The cell density was estimated from the growth dynamics experiment on agar plates. L_{th}, set as $0.1 * L_{max}$ in Fig. 5, is determined by the maximum amplitude (L_{max}) of the circuit at the end of the experiment.

All fluorescence images are flat-field corrected to compensate for uneven illumination and detection. Uniform fluorescence samples were prepared by mixing fluorescein with melted 1.5% LB agar to final concentrations of 5 nM, 10 nM and 15 nM to perform flat-field correction of different fluorescence. S_{ij} represents fluorescence intensity of the original image of the uniform sample at position (i.j). S' represents the average intensity of the original uniform sample. For each I_{ij}, original fluorescence intensity of the experiment sample, the flat-field corrected $I^f_{ij} = \frac{I_{ij} S'}{S_{ij}}$.

Self-activation measurement on agar *E. coli* strain CY027 containing the corresponding plasmids were cultured overnight. Plates were prepared using the same method as described in the signal propagation assay. Each strain had three technical replicates. All plates were allowed to solidify at room temperature for 10 minutes and incubated at 37°C. We imaged each plate under brightfield and yellow fluorescence at 10 hours.

96-well plate assays To measure the response of each strain to erythromycin, we grew the corresponding cells in liquid culture with kan and spec. The saturated culture was diluted 1/100 into fresh LB media with antibiotics and aliquoted into a 96-well plate. After shaking for 1 hour at 37C in a TECAN Spark plate reader, 100 μL of media with 2X inducer was added to the cultures. The final erythromycin concentrations

were as follows: 100 μg/mL, 30 μg/mL, 10 μg/mL, 3 μg/mL, 1 μg/mL, 0.3 μg/mL, 0.1 μg/mL, and 0 μg/mL. The plate was incubated in the plate reader for 11 hours with measurements taken every 10 minutes. The response curves in Supplementary Fig. 1a were obtained at 11 hours at which the cells reached the stationary phase.

Growth dynamics on agar plates To measure the growth dynamics of each circuit on agar plates, we developed a sample and plating assay to count the colonies. Plates were prepared using the same method as described in the signal propagation assay. We use 1000 μL pipette tips to collect three samples from the plate every hour for a total of 6 hours. The samples were immediately mixed with PBS buffer to halt growth and vigorously vortexed for 5 minutes before being serially diluted to the appropriate cell density. The dilution concentration was determined through tests to keep the cell densities between 20 and 150 per sample, ensuring that the colonies spread sufficiently for accurate counting. For each sample, 10 μL of diluted cell culture was spread on a LB agar plate with three replicates. The averaged cell count of the three replicates represents the cell count of the sample. This process was repeated for each circuit at three different initial densities, with three technical replicates.

The growth parameters of each circuit were estimated using MATLAB. We modeled the cell density $n(t)$ with the following equation proposed by Huang [41]:

$$n(t) = n_0 + n_{max} - \ln\left\{e^{n_0} + [e^{n_{max}} - e^{n_0}]e^{-\mu_{max}B(t)}B(t)\right\} \tag{6}$$

$$B(t) = t + \frac{1}{\alpha}\ln(\frac{1+e^{-\alpha(t-\lambda)}}{1+e^{\alpha\lambda}}) \tag{7}$$

where t is the time, μ_{max} is the maximum growth rate, n_0 is the natural logarithm of initial cell density, n_{max} is the natural logarithm of carrying capacity of the medium and $n(t)$ is the natural logarithm of of cell density in the medium. The average cell density we acquired from the experiment is used to estimate the growth parameters for each circuit with each initial cell density. The experimental data and fitted growth curve is shown in Supplementary Fig. 2. The estimate growth parameters from these experiments are shown in Supplementary Table 2 .

Cellular growth function In this section, we define the cell growth function $f_i(t)$ used in equation (2) for each circuit with index i. Klumpp et al. have previously established that the transcriptional rate of a protein is positively proportional to the growth rate of the cells producing them[30]. We estimate that the transcriptional rate has a square root dependence on the growth rate. From equation(4), we define a new dimensionless parameter $\rho_i \equiv n_{0,i}/C_i$. Normalizing $n_i(t)$ by the circuit-specific carrying capacity C_i, we arrive at

$$\frac{n_i(t)}{C_i} = \frac{\rho_i e^{g_i B_i(t)}}{\rho_i e^{g_i B_i(t)} + 1}. \tag{8}$$

Now we take the time derivative of the previous equation to get

$$\frac{\dot{n}_i}{C_i} = \frac{g_i \rho_i e^{g_i B_i(t)} \dot{B}_i(t)}{(\rho_i e^{g_i B_i(t)} + 1)^2}. \tag{9}$$

In our model, the growth rate is $\dot{n}_i/n_i$, therefore the transcription rate per cell is $\sqrt{\dot{n}_i/n_i}$. The total transcription rate for n_i cells at a particular location is thus proportional to $n_i\sqrt{\dot{n}_i/n_i} = \sqrt{n_i\dot{n}_i}$

$$f_i(t) \equiv \sqrt{\frac{n_i\dot{n}_i}{g_i C_i^2}} = \frac{\rho_i e^{g_i B_i(t)}\sqrt{\dot{B}_i(t)}}{(\rho_i e^{g_i B_i(t)} + 1)^{3/2}} \tag{10}$$

where $1/\sqrt{g_i}$ is introduced in the final step to make the resulting expression dimensionless.

Determination of parameters from liquid culture data To determine particular parameters for the model, we use fitted data taken from the experiments done in liquid culture. To do so, we first neglect the spatial effects of diffusion for a well mixed medium. Second, we also note that the four circuits can be categorized in two distinct groups: the IS-PF+ case is simply the addition of a responder to the control circuit and likewise for the IS+PF+ case being the quorum sensing circuit with the responder added. Hence, we can assume that in a well mixed medium, both the quorum sensing and control circuits are identical. Thus we simply write

$$\frac{dz}{dt} = af_1(t)\frac{s^H}{s^H + \tilde{s}^H} \tag{11}$$

$$\frac{dy}{dt} = \phi f_1(t)z \tag{12}$$

for the control and quorum sensing circuits where, for the sake of our argument, we have temporarily dropped the subscript labeling for each circuit and likewise temporarily renamed s_i as $\tilde{s}$. The source term s is some constant due to the medium. We solve the ordinary differential equation for $z(r,t)$:

$$z(r,t) = a\frac{s^H}{s^H + \tilde{s}^H}\int_0^t f(t')dt' \tag{13}$$

where we use a placeholder variable t' for time t. The solution of $y(r,t)$ can now be rewritten as

$$y(r,t) = \phi a\frac{s^H}{s^H + \tilde{s}^H}\int_0^t f(t')dt'\int_0^{t'} f(t'')dt'' \tag{14}$$

where we once again use a placeholder variable t'' for time. At long times y_∞, the integrals become definite and collapse into a constant

$$y_\infty = \phi a\frac{s^H}{s^H + \tilde{s}^H}\int_0^\infty f(t')dt'\int_0^{t'} f(t'')dt'' \tag{15}$$

$$y_\infty = W\phi a\frac{s^H}{s^H + \tilde{s}^H} \tag{16}$$

where W is some constant. Equation (16) indicates YFP at long times depends on s only via the activation function, implying that the liquid culture parameters s_1 and

H_1 can be directly taken from the fitted data. A similar argument is made for the quorum sensing circuit as z is uniform in liquid culture. Hence, from Supplementary Fig. 1a: $H_1 = 1.6$, $s_1 = 8.7\,\mu$g/mL, $H_3 = 1.9$, and $s_3 = 6.3\,\mu$g/mL. This leaves J_2, b_2, z_2, J_4, b_4, and z_4 as free parameters. Our choice of parameters is further explained in the following section.

Choice of other parameters We approximate the droplet size to be $R_0 = 0.5\,$mm. The diffusion constant of an eryC molecule was estimated to be $D = 500\,\mu\text{m}^2/\text{s}$. For the secondary diffusing molecule C4-HSL z, we used the fact that the molecular weight of erythromycin (733 g/mol) is about 1.6 times larger than that of C4-HSL (171 g/mol) to set the diffusivity $E \approx 1.6 \cdot D = 800\,\mu\text{m}^2/\text{s}$. We set the initial concentration as $s_0 = 2000\,\mu$g/mL as in the experiments.

Starting with the feedback only case (IS-PF+), b_2 qualitatively amplifies the strength of the of response in rhlI once the concentration threshold, z_2, is met. Hence, an increase in b_2 changes the propagation of the feedback circuit from to super-diffusive, an outcome not seen in the experiments. (Supplementary Fig. 8a) By changing z_2, we likewise change the time in which the threshold is met (Supplementary Fig. 8b). Lastly, J_i is the hill coefficient for rhlI production. In this case, J_2 sets the sharpness of the response once the threshold has been met (Supplementary Fig. 8c). A higher J_2 corresponds to a faster propagation, if the feedback begins sooner (b_2 gets smaller) and/or the threshold concentration is smaller (z_2 gets smaller). We set $b_2 = 2.5$, $J_2 = 2$, and $z_2 = 0.6\,\mu$g/mL to approximate the experimental results in Fig. 3.

For the IS+PF+ circuit, b_4, z_4, and J_4 behave qualitatively the same as previously discussed. Calibration of each parameter value was taken by approximating the experimental amplitude of the IS+PF+ circuit. Thus, we set $b_4 = 2.5$, $z_4 = 0.03\,\mu$g/mL and $J_4 = 2$ (Supplementary Fig. 8d-f).

Effects of araC degradation in signal propagation To explore the effects of the half-maximal concentration z_2 and z_4 for both the IS-PF+ and IS+PF+ cases, we incorporate the effects of degradation of araC in the positive feedback circuit. The new model with araC degradation is

$$\frac{ds}{dt} = D\left(\frac{1}{r}\frac{\partial s}{\partial r} + \frac{\partial^2 s}{\partial r^2}\right) \tag{17}$$

$$\frac{dz}{dt} = f_1(t)\left[\frac{a_1 s^{H_1}}{s^{H_1} + s_1^{H_1}} + \frac{a_1 b_2 z^{J_2}}{z^{J_2} + z_2^{J_2}}\right] - \mu z \tag{18}$$

$$\frac{dy}{dt} = f_1(t)\phi z \tag{19}$$

for the IS-PF+ strain. Here, $\mu = 10\,\text{h}^{-1}$ is the degradation rate. Supplementary Fig. 9 shows the results of having $z_2 = z_4$ with araC degradation. When degradation is included, the output of the model is similar to that of Figure 3 in the main text. Thus, we can assume that our choice of $z_2 > z_4$ is consistent with the fact that the responder protein araC also degrades as it accumulates in the circuit.

Declarations

- Data availability All data supporting the findings in the main text figures and extended data figures have been deposited in the GitHub repository at http://github.com/gonzalezlouis/Bacterial-Signal-Relay. Raw microscope images are available from the corresponding author upon reasonable request. Plasmids used in this study are available through Addgene.
- Code availability The Matlab scripts for images analysis and model simulations can be accessed via http://github.com/gonzalezlouis/Bacterial-Signal-Relay.
- Author contribution M.W., S.S., K.J., A.M. and M.R.B. conceptualized and designed the project. M.W. performed experiments and analyzed the data. L.G. and A.M. carried out the modeling and simulations. A.M., K.J. and M.R.B. oversaw the project. M.W. and L.G. drafted the manuscript, which was reviewed and revised by all authors.

Acknowledgements

This work was supported by funding from the joint National Science Foundation and National Institutes of Health Mathematical Biology Program grant 1R01GM144959 (M.W., K.J., M.R.B.), the National Science Foundation grants MCB-2118037 (L.G., S.S., A.M.), PHY-2118561 (L.G., S.S., A.M.), MCB-1936774 (M.R.B), and MCB-1936770 (K.J.), and the Welch Foundation grant C-1729 (M.R.B.).

References

[1] P. Li, M.B. Elowitz, Communication codes in developmental signaling pathways. Development **146**(12), dev170977 (2019)

[2] M. Zinner, I. Lukonin, P. Liberali, Design principles of tissue organisation: How single cells coordinate across scales. Current Opinion in Cell Biology **67**, 37–45 (2020)

[3] M. Whiteley, S.P. Diggle, E.P. Greenberg, Progress in and promise of bacterial quorum sensing research. Nature **551**(7680), 313–320 (2017)

[4] B.L. Bassler, Small talk: cell-to-cell communication in bacteria. Cell **109**(4), 421–424 (2002)

[5] Y. Yashiroda, M. Yoshida, Intraspecies cell–cell communication in yeast. FEMS Yeast Research **19**(7), foz071 (2019)

[6] F. Wu, Y. Ha, A. Weiss, M. Wang, J. Letourneau, S. Wang, N. Luo, S. Huang, C.T. Lee, L.A. David, et al., Modulation of microbial community dynamics by spatial partitioning. Nature Chemical Biology **18**(4), 394–402 (2022)

[7] S. Basu, Y. Gerchman, C.H. Collins, F.H. Arnold, R. Weiss, A synthetic multicellular system for programmed pattern formation. Nature **434**(7037), 1130–1134

(2005)

[8] Y. Chen, J.K. Kim, A.J. Hirning, K. Josić, M.R. Bennett, Emergent genetic oscillations in a synthetic microbial consortium. Science **349**(6251), 986–989 (2015)

[9] W. Kong, D.R. Meldgin, J.J. Collins, T. Lu, Designing microbial consortia with defined social interactions. Nature Chemical Biology **14**(8), 821–829 (2018)

[10] R.N. Alnahhas, M. Sadeghpour, Y. Chen, A.A. Frey, W. Ott, K. Josić, M.R. Bennett, Majority sensing in synthetic microbial consortia. Nature Communications **11**(1), 3659 (2020)

[11] Y. Combarnous, T.M.D. Nguyen, Cell communications among microorganisms, plants, and animals: origin, evolution, and interplays. International Journal of Molecular Sciences **21**(21), 8052 (2020)

[12] S. Mukherjee, B.L. Bassler, Bacterial quorum sensing in complex and dynamically changing environments. Nature Reviews Microbiology **17**(6), 371–382 (2019)

[13] E.C. Pesci, J.B. Milbank, J.P. Pearson, S. McKnight, A.S. Kende, E.P. Greenberg, B.H. Iglewski, Quinolone signaling in the cell-to-cell communication system of pseudomonas aeruginosa. Proceedings of the National Academy of Sciences **96**(20), 11229–11234 (1999)

[14] D.P. Arora, S. Hossain, Y. Xu, E.M. Boon, Nitric oxide regulation of bacterial biofilms. Biochemistry **54**(24), 3717–3728 (2015)

[15] Y. Cao, M.D. Ryser, S. Payne, B. Li, C.V. Rao, L. You, Collective space-sensing coordinates pattern scaling in engineered bacteria. Cell **165**(3), 620–630 (2016)

[16] L. Gelens, G.A. Anderson, J.E. Ferrell Jr, Spatial trigger waves: positive feedback gets you a long way. MBoC **25**(22), 3486–3493 (2014)

[17] A. Prindle, J. Liu, M. Asally, S. Ly, J. Garcia-Ojalvo, G.M. Süel, Ion channels enable electrical communication in bacterial communities. Nature **527**(7576), 59–63 (2015)

[18] J.B. Chang, J.E. Ferrell Jr, Mitotic trigger waves and the spatial coordination of the xenopus cell cycle. Nature **500**(7464), 603–607 (2013)

[19] H.K. Co, C.C. Wu, Y.C. Lee, S.h. Chen, Emergence of large-scale cell death through ferroptotic trigger waves. Nature pp. 1–9 (2024)

[20] P.B. Dieterle, J. Min, D. Irimia, A. Amir, Dynamics of diffusive cell signaling relays. Elife **9**, e61771 (2020)

[21] K. Patel, C. Rodriguez, E.V. Stabb, S.J. Hagen, Wavelike propagation of quorum activation through a spatially distributed bacterial population under natural regulation. Phys. Biol. **18**(4), 046008 (2021)

[22] M.K. Kim, F. Ingremeau, A. Zhao, B.L. Bassler, H.A. Stone, Local and global consequences of flow on bacterial quorum sensing. Nature Microbiology **1**(1), 1–5 (2016)

[23] S.E. Darch, O. Simoska, M. Fitzpatrick, J.P. Barraza, K.J. Stevenson, R.T. Bonnecaze, J.B. Shear, M. Whiteley, Spatial determinants of quorum signaling in a pseudomonas aeruginosa infection model. Proceedings of the National Academy of Sciences **115**(18), 4779–4784 (2018)

[24] K. Papenfort, B.L. Bassler, Quorum sensing signal–response systems in gram-negative bacteria. Nature Reviews Microbiology **14**(9), 576–588 (2016)

[25] K. Showalter, J.J. Tyson, Luther's 1906 discovery and analysis of chemical waves. Journal of Chemical Education **64**(9), 742 (1987)

[26] J.J. Tyson, J.P. Keener, Singular perturbation theory of traveling waves in excitable media (a review). Physica D: Nonlinear Phenomena **32**(3), 327–361 (1988)

[27] G.E. Dilanji, J.B. Langebrake, P. De Leenheer, S.J. Hagen, Quorum activation at a distance: spatiotemporal patterns of gene regulation from diffusion of an autoinducer signal. Journal of the American Chemical Society **134**(12), 5618–5626 (2012)

[28] K. Patel, C. Rodriguez, E.V. Stabb, S.J. Hagen, Spatially propagating activation of quorum sensing in vibrio fischeri and the transition to low population density. Phys. Rev. E **101**(6), 062421 (2020)

[29] T. Danino, O. Mondragón-Palomino, L. Tsimring, J. Hasty, A synchronized quorum of genetic clocks. Nature **463**(7279), 326–330 (2010)

[30] S. Klumpp, Z. Zhang, T. Hwa, Growth rate-dependent global effects on gene expression in bacteria. Cell **139**(7), 1366–1375 (2009)

[31] M. Scott, C.W. Gunderson, E.M. Mateescu, Z. Zhang, T. Hwa, Interdependence of cell growth and gene expression: origins and consequences. Science **330**(6007), 1099–1102 (2010)

[32] A.J. Meyer, T.H. Segall-Shapiro, E. Glassey, J. Zhang, C.A. Voigt, Escherichia coli "marionette" strains with 12 highly optimized small-molecule sensors. Nature Chemical Biology **15**(2), 196–204 (2019)

[33] E.C. Pesci, J.P. Pearson, P.C. Seed, B.H. Iglewski, Regulation of las and rhl quorum sensing in pseudomonas aeruginosa. Journal of Bacteriology **179**(10), 3127–3132 (1997)

[34] J.M. Ho, C.A. Miller, S.E. Parks, J.R. Mattia, M.R. Bennett, A suppressor trna-mediated feedforward loop eliminates leaky gene expression in bacteria. Nucleic Acids Res. **49**(5), e25–e25 (2021)

[35] J.B. Andersen, C. Sternberg, L.K. Poulsen, S.P. Bjørn, M. Givskov, S. Molin, New unstable variants of green fluorescent protein for studies of transient gene expression in bacteria. Applied and Environmental Microbiology **64**(6), 2240–2246 (1998)

[36] P. Pletnev, I. Osterman, P. Sergiev, A. Bogdanov, O. Dontsova, Survival guide: Escherichia coli in the stationary phase. Acta Naturae ( ) **7**(4 (27)), 22–33 (2015)

[37] J.M. Navarro Llorens, A. Tormo, E. Martínez-García, Stationary phase in gram-negative bacteria. FEMS Microbiology Reviews **34**(4), 476–495 (2010)

[38] R. Schleif, Regulation of the l-arabinose operon of escherichia coli. Trends in Genetics **16**(12), 559–565 (2000)

[39] M. Gao, H. Zheng, Y. Ren, R. Lou, F. Wu, W. Yu, X. Liu, X. Ma, A crucial role for spatial distribution in bacterial quorum sensing. Scientific Reports **6**(1), 34695 (2016)

[40] S. Alberghini, E. Polone, V. Corich, M. Carlot, F. Seno, A. Trovato, A. Squartini, Consequences of relative cellular positioning on quorum sensing and bacterial cell-to-cell communication. FEMS Microbiology Letters **292**(2), 149–161 (2009)

[41] L. Huang, A new mechanistic growth model for simultaneous determination of lag phase duration and exponential growth rate and a new bělehrádek-type model for evaluating the effect of temperature on growth rate. Food Microbiology **28**(4), 770–776 (2011)

[42] A. Cooper, A. Dean, C.N. Hinshelwood, Factors affecting the growth of bacterial colonies on agar plates. Proceedings of the Royal Society of London. Series B. Biological Sciences **171**(1023), 175–199 (1968)

[43] X. Shao, A. Mugler, J. Kim, H.J. Jeong, B.R. Levin, I. Nemenman, Growth of bacteria in 3-d colonies. PLoS Computational Biology **13**(7), e1005679 (2017)

[44] B.P. Landry, R. Palanki, N. Dyulgyarov, L.A. Hartsough, J.J. Tabor, Phosphatase activity tunes two-component system sensor detection threshold. Nature Communications **9**(1), 1433 (2018)

[45] A.L. Todeschini, A. Georges, R.A. Veitia, Transcription factors: specific dna binding and specific gene regulation. Trends in Genetics **30**(6), 211–219 (2014)

[46] F.W. Studier, B.A. Moffatt, Use of bacteriophage t7 rna polymerase to direct selective high-level expression of cloned genes. Journal of Molecular Biology **189**(1), 113–130 (1986)

[47] A. Tabib-Salazar, B. Liu, D. Barker, L. Burchell, U. Qimron, S.J. Matthews, S. Wigneshweraraj, T7 phage factor required for managing rpos in escherichia coli. Proceedings of the National Academy of Sciences **115**(23), E5353–E5362 (2018)

[48] R. Hengge-Aronis, Signal transduction and regulatory mechanisms involved in control of the σs (rpos) subunit of rna polymerase. Microbiology and Molecular Biology Reviews **66**(3), 373–395 (2002)

[49] S. Lacour, P. Landini, σs-dependent gene expression at the onset of stationary phase in escherichia coli: function of σs-dependent genes and identification of their promoter sequences. Journal of Bacteriology **186**(21), 7186–7195 (2004)

[50] T. Shimada, H. Makinoshima, Y. Ogawa, T. Miki, M. Maeda, A. Ishihama, Classification and strength measurement of stationary-phase promoters by use of a newly developed promoter cloning vector. Journal of Bacteriology **186**(21), 7112–7122 (2004)

[51] L. Tripathi, Y. Zhang, Z. Lin, Bacterial sigma factors as targets for engineered or synthetic transcriptional control. Frontiers in Bioengineering and Biotechnology **2**, 33 (2014)

[52] O. Baghdasaryan, J. Lee-Kin, C. Tan, Architectural engineering of cyborg bacteria with intracellular hydrogel. Materials Today Bio **28**, 101226 (2024)

[53] A. Rodrigo-Navarro, S. Sankaran, M.J. Dalby, A. del Campo, M. Salmeron-Sanchez, Engineered living biomaterials. Nature Reviews Materials **6**(12), 1175–1190 (2021)

[54] B. An, Y. Wang, Y. Huang, X. Wang, Y. Liu, D. Xun, G.M. Church, Z. Dai, X. Yi, T.C. Tang, et al., Engineered living materials for sustainability. Chemical Reviews **123**(5), 2349–2419 (2022)